Chapter 2
X-Ray Projection Imaging

Abstract X-ray imaging is the oldest medical imaging modality, which found its way into medical practice shortly after the discovery of the X-rays in 1895. X-ray imaging is a projection technique, and image formation takes place traditionally on photosensitive film, although direct digital X-ray imaging is becoming more and more common. In its most common form, X-ray imaging is a qualitative modality. X-rays are high-energy photons, and atomic interaction with inner shell electrons is fundamental to both X-ray production and generation of X-ray contrast. Soft-tissue contrast is comparatively low, but bone and air provide excellent contrast. In some cases, contrast can be enhanced with contrast agents. An undesirable (but unavoidable) side-effect of the photon-atom interaction is the ionization of tissue along the beam path, which can lead to radiation damage. X-ray images can reveal very subtle features, and its popularity is further enhanced by the relatively inexpensive equipment and the straightforward imaging procedure.

2.1 X-Ray Generation

X-rays are generated when kinetic electrons interact with a solid target and undergo sudden deceleration ("braking radiation" or "bremsstrahlung"). As electrons lose some of their kinetic energy, this energy is released as an X-ray photon. In an X-ray tube, electrons are emitted into the vacuum at the cathode and accelerated toward the anode in a high-voltage electrostatic field. In the dense metallic anode material, the electrons lose part of their energy when they are deflected in the Coulombic field of the nucleus (Fig. 2.1). The extreme case is a direct collision of a high-energy electron with a nucleus, whereby the electron loses all of its kinetic energy, and a photon of the same energy is emitted. If the electron comes in close proximity of the nucleus, it is deflected by electrostatic forces. In the process, the electron loses some (but not all) of its energy, and a photon is emitted that carries this amount of energy. The greater the distance to the nucleus, the lower the energy loss of the electron and the lower the photon energy. Electrons can undergo multiple interactions with

M. A. Haidekker, *Medical Imaging Technology*, SpringerBriefs in Physics,
DOI: 10.1007/978-1-4614-7073-1_2, © The Author(s) 2013

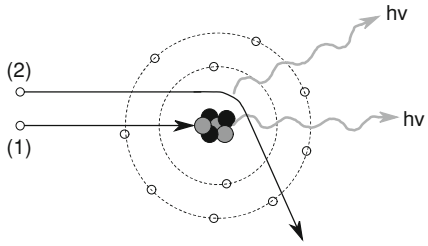

Fig. 2.1 X-ray generation by electron deceleration. High-energy electrons come in proximity of a nucleus of the anode material and are deflected in the Coulombic field of the nucleus. In the extreme case (*1*), the electron collides directly with the nucleus, thereby releasing all of its kinetic energy into one X-ray photon. A close "fly-by" (*2*) is much more probable, but the electron loses less energy, and the resulting X-ray photon has a lower energy and a correspondingly longer wavelength

nuclei before they expend all of their energy. Since the kinetic energy E_{kin} of the electrons only depends on the electrostatic potential (i.e., the anode voltage U), the maximum photon energy E_{max} and its corresponding shortest wavelength λ_{min} can be computed as

$$E_{\text{kin}} = \frac{1}{2} m_e v^2 = e \cdot U \tag{2.1}$$

$$E_{\text{kin}} = E_{\text{max}} = \frac{hc}{\lambda_{\text{min}}} \tag{2.2}$$

where m_e is the electron mass, e its charge, v its velocity upon impact with the anode, h is Planck's constant, and c the speed of light.

The X-ray radiation generated in a regular X-ray tube has therefore a continuous energy *spectrum*. A direct collision with the nucleus is rare, and photons with the highest possible energy occur in the spectrum with a low probability. The probability increases with increasing electron-nucleus distance and correspondingly lower photon energy.

Interactions of the high-energy electrons with shell electrons of the anode material play a significant role. If high-energy electrons collide with shell electrons, the atom of the anode material can be excited or ionized, usually by ejection of a k-shell electron. As the k-shell vacancy gets filled, energy is released—again as X-ray radiation. Since the binding energies of the target material are fixed, the X-ray energy that is emitted from shell electrons has a very narrow energy spectrum (Fig. 2.2). These narrow spikes in the energy spectrum are referred to as *characteristic X-rays*, because they are characteristic for the target material.

Example: In a tube with a tungsten anode, the anode voltage is 75 kV. The highest possible energy is 75 keV (1 eV $= 1.602 \times 10^{-19}$ J). The shortest wavelength $\lambda_{\text{min}} =$ 16.5 pm (pm = picometers $= 10^{-12}$ m). In addition, the binding energy of the k-shell electrons of tungsten is 69.5 keV, and the binding energy of the l-shell electrons is 12.1 keV. If an electron is ejected from the k-shell, and the vacancy is filled from the

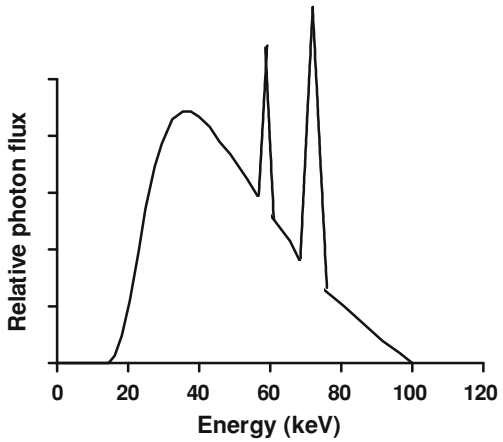

Fig. 2.2 Typical X-ray spectrum of a tube with a tungsten anode operated at 100 kV. The maximum possible photon energy is 100 keV, but lower energies are more probable. Very low energies (25 keV and below) get absorbed by the anode material and by the glass wall of the tube, and do not occur in the spectrum. Two prominent peaks of characteristic X-rays can be seen at 69.5 keV (k-shell) and 57.4 keV (k−l transition)

l-shell, the energy difference of 57.4 keV is emitted as an X-ray photon. Note that the binding energy of higher shells is too low to cause X-ray radiation. Note also that the characteristic X-ray radiation can only occur if the kinetic energy of the incident electrons is high enough to allow at least the k−l transition. For example, if the tube is operated at 50 kV, no characteristic X-rays from tungsten can be seen.

For comparison, visible light (green) has a wavelength of 520 nm and an associated energy of 2.4 eV. The lowest energy to affect the atomic shell is the k−l excitation of hydrogen and requires 10.1 eV with an associated wavelength of 123 nm. Diagnostic X-rays lie approximately in the range from 30 to 120 keV with wavelengths in the picometer range.

2.1.1 The X-Ray Tube

The actual X-ray tube consists of a vacuum glass cylinder with the anode and cathode inside. Electrical contacts allow connecting of the cathode, its heating filament, and the anode to the power sources. The anode is usually made of copper for good heat conduction with a small target area of tungsten or rhodium. Tungsten melts at about 3700 K, and copper has a melting point of about 1360 K. Heat dissipation is important, because only a small amount of the electron beam's kinetic energy is actually emitted as X-rays. X-ray tubes have a fairly poor degree of efficiency η, which can be approximated by

$$\eta = k \cdot U \cdot Z \tag{2.3}$$

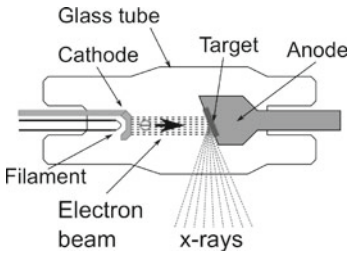

Fig. 2.3 Schematic representation of an X-ray tube. The cathode is heated by the filament, and electrons are ejected into the vacuum by thermionic emission. These electrons are accelerated by the electrostatic field between anode and cathode. As the electrons hit the target material of the anode, they emit X-ray radiation by deceleration. The anode is usually a massive body of metal to facilitate heat transport from the target to the outside of the tube

where k is a proportionality constant with approximately $k = 1.1 \times 10^{-9}$, U is the anode voltage, and Z is the atomic number of the anode material, for example, $Z = 74$ for tungsten. Typically, about 1 % of the energy is emitted as X-rays, and 99 % is lost as heat. Assuming a 70 kV tube with a tube current of 5 mA, total energy dissipation is 350 W, comparable to a hair dryer on a medium setting. For this reason, large X-ray tubes designed for continuous operation use rotating anodes: the anode is a large disc, driven by a motor. The disc is beveled, and electrons hit only a small active region on the beveled rim. The rotating anode shows much lower local heating than a fixed anode.

The cathode is heated by a filament, and electrons are injected into the vacuum by thermionic emission. Electrons from the cathode are accelerated toward the anode, gathering kinetic energy in the process. When the electrons hit the target material of the anode, they lose their kinetic energy, and X-rays are emitted.

A simplified sketch of an X-ray tube is shown in Fig. 2.3. The anode target is usually angled to direct a large part of the X-ray radiation perpendicular to the electron beam.

The filament current allows to control the cathode temperature. The thermionic effect is highly temperature dependent, and the current flux S (current per area unit of emitting cathode material) is described by the *Richardson equation*,

$$S = A_{\mathrm{R}} \cdot T^2 \cdot \exp\left(-\frac{E_{\mathrm{A}}}{\mathrm{k}T}\right) \tag{2.4}$$

where A_{R} is the Richardson constant, E_{A} is the activation energy (also called work function), k is Boltzmann's constant, and T is the absolute temperature. A_{R} and E_{A} are material constants of the cathode material. To achieve a reasonable tube current, a cathode temperature between 1800 and 2000 K is desirable (Fig. 2.4). Special cathode materials, such as cesium on tungsten or barium oxide, have a lower activation energy and require lower temperatures for the desired tube current. The activation energy

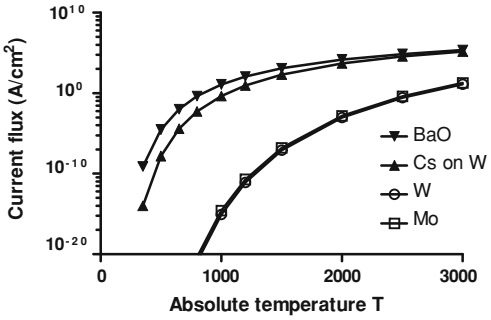

Fig. 2.4 Temperature-dependency of the cathode current flux by thermionic emission (Eq. 2.4). Typical tube currents are in the milliampere range, and a tungsten cathode needs to be heated to near its melting point. Some special materials, such as cesium or barium oxide, have a lower activation energy and require lower temperatures

Table 2.1 Richardson constant A_R and activation energy E_A of some cathode materials

Material	E_A (eV)	A_A (A / cm^2 K^2)
Tungsten	4.53	60
Molybdenum	4.43	55
Cs on W	1.36	3.2
BaO	0.99	1.18

E_A and Richardson constant A_R for some common cathode materials is listed in Table 2.1.

The X-ray tube has two main "knobs" which influence the emitted radiation (see also Fig. 2.5):

1. The anode voltage: Increasing the anode voltage increases the maximum energy of the X-ray photons, and it also increases the total number of photons emitted. An empirical relationship between the anode voltage U and the number of photons emitted N is
$$N = \mathrm{k} \cdot Z \cdot U^m \tag{2.5}$$
where k is a tube-dependent proportionality constant, Z is the atomic number of the target material, and m is a material-dependent exponent, typically $m \approx 2$.
2. The tube current: By modifying the filament current and with it the cathode temperature, the tube current can be controlled. Increasing the tube current by increasing the filament temperature increases X-ray photon flux, but does not change the highest energy of the emitted photons.

In practice, the X-ray tube is housed in a lead-shielded assembly to prevent X-ray radiation in any direction except the aperture of the X-ray housing. Often, collimators (movable lead blades) allow adjustment of the aperture. With a suitably positioned

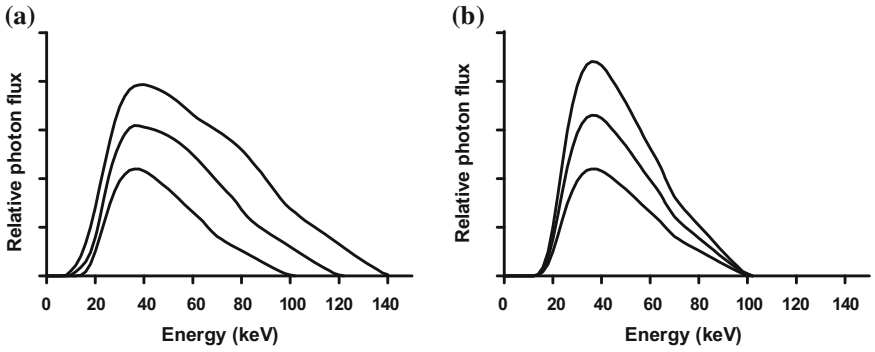

Fig. 2.5 Qualitative changes of the emission spectra (characteristic X-rays omitted!) of an X-ray tube when the anode voltage is increased (**a**) and when the filament current is increased (**b**). An increase of the anode voltage (in this example from 100 to 120 and 140 kV) increases the maximum photon energy, but indirectly also increases the tube current and therefore the total photon flux. Conversely, an increase of the filament current (in this example by 20 and 50 %) increases the total photon flux, but not their energy distribution. Notably, the maximum energy remains the same

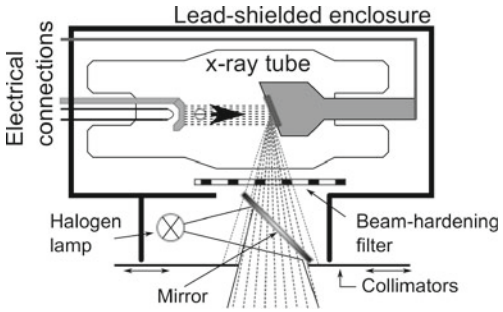

Fig. 2.6 Schematic representation of an X-ray tube assembly with its enclosure and additional features. A beam-hardening filter removes low-energy X-rays from the beam. Subsequently, movable collimators allow control of the illuminated area. A visible-light lamp and a mirror provide visual information on the illuminated area. The entire enclosure is heavily lead-shielded to minimize radiation everywhere except at the target area of the patient

lamp and mirror, the area that will be exposed to X-rays can be highlighted beforehand with visible light. Lastly, a beam-hardening filter (sometimes removable) absorbs some of the low-energy radiation and reduces the patient dose. Figure 2.6 shows a sketch of a complete X-ray tube assembly with its housing, beam-hardening filter, collimators, and guide lamp.

A complete X-ray generator contains several more components. The key element is the high-voltage generator, built around a transformer and frequently a high-voltage cascade, such as a Cockroft-Walton multiplier. Through a resistor voltage divider, the anode voltage can be measured. For example, if the voltage divider has a ratio of 1:10,000, an anode voltage of 150 kV is converted down to 15 V, which is in

the voltage range of conventional operational amplifiers. A closed-loop feedback control system is therefore feasible that tightly controls the anode voltage. Similarly, a current shunt resistor allows to measure the tube current and, through a feedback control system, to control the filament current. In addition, the total dose emitted by the X-ray tube can be measured and used to shut off the high voltage after the exposure is finished. Selection of the exposure time adds a third "knob", but tube current and exposure time have similar effects.

2.1.2 A Focus on Geometry

The anode is usually angled to direct a large part of the X-ray radiation perpendicular to the electron beam. Moreover, the anode angle allows to balance illumination strength of the tube with its ability to resolve small details. The cathode emits an electron beam of diameter d (Fig. 2.7). The projected focal spot, as seen from the detector, has a diameter $D = d / \tan \alpha$. Both the anode angle α and the electron beam diameter d are design parameters:

- A thin electron beam with a small diameter d has a small focal spot with good detail resolution, but poor overall intensity, because the maximum tube current is limited.
- An electron beam with a large diameter d and a steep angle $\alpha \rightarrow 90°$ also has a small focal spot, but larger tube currents are possible. Because of the large angle, however, the illuminated field is limited.
- An electron beam with a large diameter d and a small angle α has a large focal spot with poor detail resolution (details are *blurred*). However, larger tube currents are possible, and a wide field of illumination can be achieved.

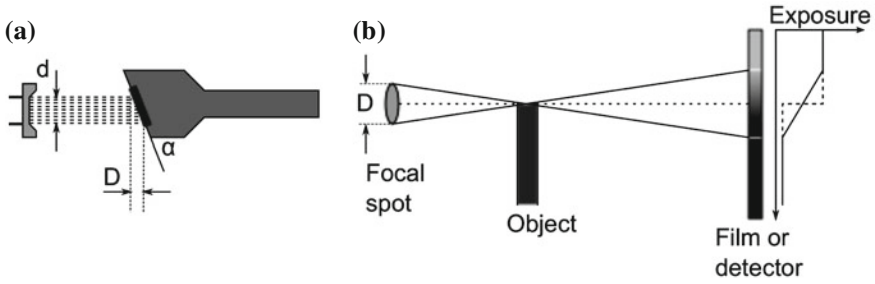

Fig. 2.7 Relevance of the focal spot size. **a** The anode angle α relates the focal spot (i.e., the diameter of the electron beam d) to the projected focal spot size D through $D = d / \tan \alpha$. The focal spot size limits the size of small details that can be discerned in the image. **b** With an idealized point source, the edge of any radio-opaque object leads to a steep transition of the exposure at the detector. When the focal spot is large, a transition zone appears, in which the sharp edge appears blurred on the detector

A small field of illumination is sometimes desirable, for example, for pencil-beam CT tubes. In many cases, the emphasis lies on a small focal spot, for example for dental X-rays. Several designs exist where the size of the focal spot can be adjusted, for example, by providing a cathode with two emitters (Wehnelt cylinders): a wide field illumination with a large focal spot can be used for scout images, and by switching to the fine-focus cathode, a sharper image of a smaller zone of interest can be taken.

2.2 X-Ray Attenuation

We will now examine the source of X-ray *contrast*: the absorption of X-rays in matter of different density and composition. We will first examine the mechanisms of absorption on the atomic scale, and then create a macroscopic model of absorption. High-energy X-ray photons lose some or all of their energy in a collision with atoms along their path. Often, the photon is deflected from its path, i.e., scattered. In addition, the high-energy photons can elevate shell electrons to a higher energy level, causing either *excitation* or *ionization*:

- *Ionization* occurs when an electron is ejected from the atom into the continuum. Since the electron is completely ejected, the atom is positively charged (an ion) until the electron vacancy is filled. Ionization requires energy (namely, the binding energy of the electron's shell), and filling the vacancy releases this energy again (photon).
- *Excitation* occurs when an electron—most often a k-shell electron—is elevated to an outer shell. Excitation requires energy, namely, the binding energy difference between the two shells. When the vacancy in the inner shell is filled, the energy is released again (photon). Since the electron remains in one of the atomic shells, the excited atom does not carry a charge (i.e, does not become an ion).

2.2.1 Photon-Matter Interaction

An X-ray photon can interact with matter in any of the following four ways:

1. *Rayleigh scattering*. This is an elastic collision of the photon with the atom that occurs predominantly at low photon energies. The collision causes the atoms to vibrate, and the photon loses a small portion of its energy. Scattering occurs at a small deflection angle. The rate of Rayleigh scattering rapidly diminishes with increasing X-ray energy, and Rayleigh scattering plays a negligible role in the diagnostic range from 50 keV upward.
2. *Compton scattering*. Compton scattering is the dominant interaction in a wide range of photon energies. In this type of interaction, the X-ray photon ejects an electron (ionization), and the X-ray photon loses the amount of energy needed to ionize the atom. The photon can be deflected by a large angle. Filling of

the shell vacancy generates additional X-ray photons that lead to the typical energy peaks of characteristic radiation. These photons are emitted in a random direction. Compton scattering is undesirable in the imaging process, because it causes ionization along the X-ray path, and because of the unpredictable large-angle deflection of the photon, which leads to background haze and therefore lowered contrast.

3. *Photoelectric effect*. The photoelectric effect is the most important interaction for image formation. In this type of interaction, the energy of the X-ray photon is *completely* expended for ejecting and accelerating an electron (ionization) as sketched in Fig. 2.8. The kinetic energy of the electron is $m_e v^2/2 = E_{\text{photon}} - E_{\text{shell}}$. The ejected electron can have a high kinetic energy and cause additional ionization (Auger electron) and X-ray production through deceleration. Filling of the ion vacancy generates characteristic radiation. The photoelectric effect diminishes rapidly with higher energies, but dominates in the diagnostic range from 50 to 70 keV. The X-ray absorption rate of the photoelectric effect depends directly on the density of the matter. Moreover, the photon is not scattered. Therefore, the photoelectric effect is the most important contributor to X-ray contrast.
4. *Pair production*. At very high energies (above 1.02 MeV) the photon can spontaneously transform into a positron–electron pair upon colliding with an atom. This process is a total energy-matter conversion, and the energy needed is the equivalent of two electron masses: $E_{\text{photon}} = 2m_e c^2$. Since the energy needed for pair production is far above the diagnostic energy range, pair production does not play a role in diagnostic imaging.

In Fig. 2.9, we can see the contribution of the individual scattering events to the total absorption. At low energies, the total attenuation coefficient is very high, and most of the low-energy radiation gets absorbed by the patient. At high energies, Compton scattering becomes dominant, leading to poor contrast and to haze. A good energy range for diagnostic imaging is in the range from 50 to 80 keV, and for some applications, such as CT, even up to 150keV.

The ability of X-ray photons to create ions along their path—either through Compton scattering or through the photoelectric effect—is the cause of radiation damage and radiation burns. Molecules, particularly organic molecules, become more reactive when one or more of their atoms are ionized. These reactive species have a higher tendency to break apart or to react with nearby molecules. Cells can repair a certain amount of damage and therefore resist the influence of background radiation and low levels of radiation exposure. When radiation exposure exceeds the ability of the cell's repair mechanism, cells sustain irreparable damage and are replaced much like normal wound healing. If the damage exceeds the self-healing ability of the tissue, the tissue or organ may fail. Independently, ionization puts DNA elements at risk of breaking apart, which increases the probability of cancer development.

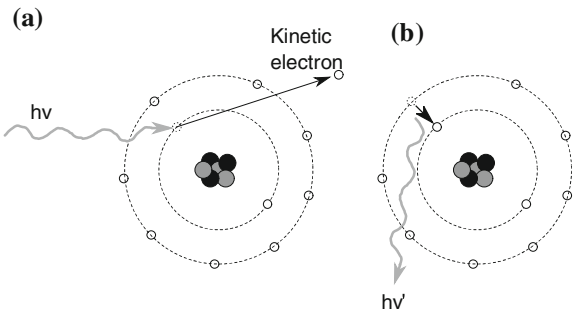

Fig. 2.8 Illustration of the photoelectric effect. **a** A high-energy X-ray photon expends all of its energy by elevating an inner-shell electron into the continuum. The difference between the photon energy and the binding energy becomes the kinetic energy of the electron. Note that this electron can have a high enough kinetic energy to cause braking radiation X-rays. Furthermore, the inner-shell vacancy is filled (**b**), which releases characteristic -rays

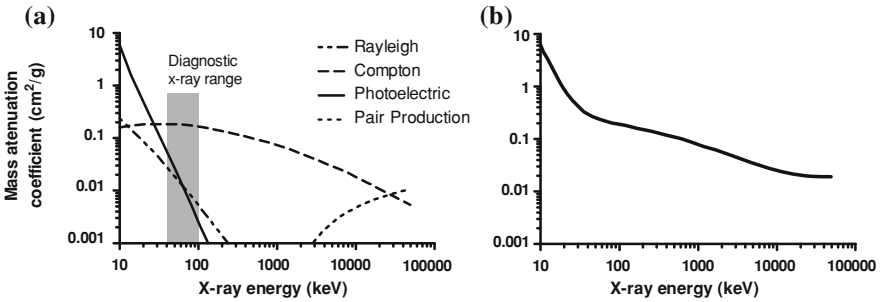

Fig. 2.9 **a** Contribution of the individual absorption events to the total X-ray absorption in a tissue-equivalent material, and **b** total absorption as the sum of the four contributing absorption events. Rayleigh scattering and photoelectric effect dominate at small energies. At extremely high energies far above the diagnostic energy range, pair production becomes dominant. Compton scattering is present over a wide range of energies. The ideal energy range for diagnostic purposes (highlighted in *gray*) exists where absorption is low enough for the majority of the photons to pass through the object, but where the photoelectric effect still contributes strongly to the total absorption. The energy-dependence of the total absorption can clearly be seen

2.2.2 Macroscopic Attenuation and Lambert-Beer's Law

We know that photons get absorbed when they pass through matter. On a macroscopic scale, the absorption manifests itself as the linear attenuation coefficient μ, usually given in cm^{-1} or the mass attenuation coefficient μ/ρ, given in cm^2/g. The two coefficients are related by the material density ρ. The absorption behavior is governed by Lambert-Beer's law, which can be derived by considering a very thin slice of absorbing material (thickness $\Delta x \to 0$). From N incident photons, Δn photons are absorbed. Δn is proportional to (a) the number of incident photons, (b) the thickness

Δx, and (c) the linear absorption coefficient μ:

$$\Delta n = N \cdot \mu \cdot \Delta x \tag{2.6}$$

If the slice is thick, N becomes a function of x, because each infinitesimal layer of material has its own incident number of photons, $N(x)$. In other words, the number of absorbed photons $\mathrm{d}N(x)/\,\mathrm{d}x$ is proportional to the number of incident photons at that location, $N(x)$, and the absorption coefficient μ. We obtain a first-order differential equation for N:

$$\frac{\mathrm{d}N(x)}{\mathrm{d}x} = -\mu \cdot N(x) \tag{2.7}$$

To solve the differential equation, we rearrange Eq. 2.7:

$$\frac{\mathrm{d}N(x)}{N(x)} = -\mu \cdot \mathrm{d}x \tag{2.8}$$

Now, Eq. 2.8 can be integrated from $x = 0$ to the length of the material l under the boundary condition that the incident number of photons at $x = 0$ is N_0:

$$\ln N(l) - \ln N_0 = -\mu l \tag{2.9}$$

Solving Eq. 2.9 for $N(l)$ yields Lambert-Beer's law [1]:

$$N(l) = N_0 \cdot e^{-\mu l} \tag{2.10}$$

The attenuation coefficient is always a function of the photon energy, that is, $\mu(E)$. The energy-dependency of the mass attenuation coefficient for three relevant tissues (muscle, adipose tissue, and bone) is shown in Fig. 2.10. In many cases, it is sufficient to approximate the tissue by some effective attenuation coefficient. However, for the quantitative determination of μ by absorption measurement, beam hardening effects need to be taken into account. *Beam hardening* refers to a shift of the peak energy toward higher energies due to stronger absorption of X-ray photons at lower energies. In the example of Fig. 2.11 with aluminum filters of 2, 5, and 10 mm thickness, the overall photon flux is reduced by 21, 39, and 59 %, respectively. However, the photon flux of photons above 80 keV is only reduced by 9, 21, and 38 %, respectively. The shift of the energy peak toward higher energies can clearly be seen.

Beam hardening effects are of minor importance in planar X-ray imaging, but can cause major artifacts in computed tomography. For this reason, beam hardening filters are used that absorb some of the low-energy radiation (see Fig. 2.6). Beam

[1] In optics, the base-10 logarithm is frequently used (e.g., the molar extinction coefficient ε of a fluid), whereas X-ray absorption coefficients μ use base-e logarithms. This is a common source of confusion.

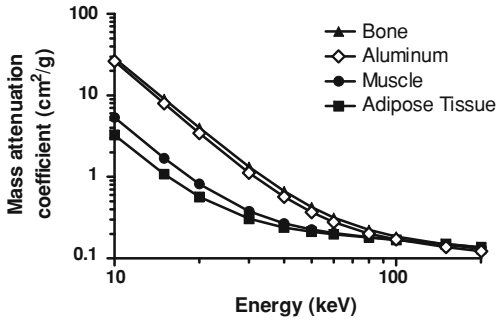

Fig. 2.10 Mass attenuation coefficient μ/ρ for muscle, adipose tissue, compact bone, and, for comparison purposes, aluminum [8]. X-ray imaging shows superior contrast between tissue and bone, but contrast between different types of tissue is relatively low

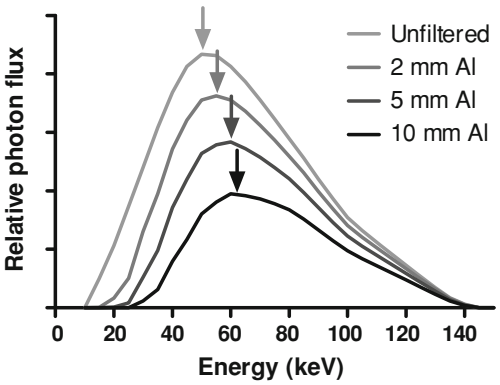

Fig. 2.11 Effect of beam hardening. Shown is the sample spectrum (characteristic X-rays omitted) of a tube at 140 keV (Fig. 2.5) and the filtered spectra after 2, 5, and 10 mm of aluminum. Arrows highlight the energy maximum.

Table 2.2 Linear attenuation coefficients (approximate) of some materials and biological tissues at 50 keV

Tissue/ material	Linear attenuation coefficient (cm^{-1})
Air	0.00029
Water	0.214
Blood	0.241
Adipose tissue	0.193
Muscle	0.226
Brain	0.237
Compact bone	0.573

hardening filters are thin films of metal that preferentially absorb the lower-energy photons.

Table 2.2 lists the linear attenuation coefficients of some materials and biological tissues at 50 keV. The large difference between bone and other biological tissues is particularly prominent. The absorption coefficients of other tissues, e.g., blood, muscle tissue, or brain matter, are very similar, and X-ray imaging provides excellent bone-tissue contrast, but poor tissue-tissue contrast.

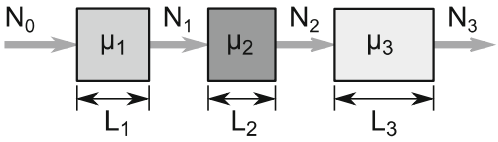

Fig. 2.12 X-ray absorption in three blocks of material of different size and different absorption coefficients

2.2.3 Lambert-Beer's Law in Inhomogeneous Materials

Equation 2.10 assumes a constant absorption coefficient along the path length l. What does Lambert-Beer's law look like in inhomogeneous materials? Figure 2.12 shows an X-ray beam attenuated by three consecutive blocks of material with different length L_i and different absorption coefficient μ_i with $i \in [1, 2, 3]$. If we assume the incident number of photons to be N_0, we can compute the non-absorbed photons N_1 entering the second block:

$$N_1 = N_0 \cdot e^{-\mu_1 L_1} \tag{2.11}$$

For the second and third block, we apply Eq. 2.10 in a similar manner:

$$\begin{aligned} N_2 &= N_1 \cdot e^{-\mu_2 L_2} \\ N_3 &= N_2 \cdot e^{-\mu_3 L_3} \end{aligned} \tag{2.12}$$

By combining the three attenuation equations into one, we can see that the exponential factors are multiplied, or the exponents added:

$$N_3 = N_0 \cdot e^{-\mu_1 L_1 - \mu_2 L_2 - \mu_3 L_3} \tag{2.13}$$

It does not matter if the materials are separated by air gaps or contiguous—the overall absorption remains the same. For the continuous case of attenuation by an inhomogeneous material along a path s, we can write the general form of Lambert-Beer's law as

$$N = N_0 \cdot \exp\left(-\int_s \mu(\sigma)\, \mathrm{d}\sigma\right) \tag{2.14}$$

where $\mu(\sigma)$ is the attenuation coefficient at any point σ of the path s.

We need to understand X-ray imaging as *projection imaging*. The X-ray image is two-dimensional, and information in one spatial dimension is lost. Let us assume that the object (patient) can be described by the absorption $\mu(x, y, z)$ as a function of the three spatial dimensions x, y, and z. Let us further make the two simplifying assumptions that (1) the image plane is the x-y-plane, and (2) that the X-ray illumination is homogeneous and approximately parallel to the z-axis. In this case, the image $I(x, y)$ that represents the detector exposure relates to the object through

$$I(x, y) \propto \exp\left(-\int_z \mu(x, y, z)\, \mathrm{d}z\right) \tag{2.15}$$

In reality, the geometry is more complex, because the X-ray source emits rays in a cone-shaped configuration, and scattered photons create a background haze that reduces overall contrast. Moreover, the incident intensity is inhomogeneous within the cone. Lastly, the detectors, most notably film, often have a nonlinear characteristic. For these reasons, conventional X-ray imaging is widely qualitative, and it requires an experienced radiologist to identify the features of interest and make a diagnosis.

2.2.4 Dual-Energy X-Ray Absorptiometry

One area where projection X-ray imaging is used for highly accurate quantitative measurements is DEXA (dual-energy X-ray absorptiometry), usually used to measure bone density to diagnose osteopenia or osteoporosis. DEXA scanners are accurately calibrated, and the incident photon flux is either homogeneous or its spatial distribution known. DEXA operates under the assumption of a two-component model, i.e., that X-rays are attenuated along the path by either bone or soft tissue: When an X-ray beam travels through both bone and soft tissue, Eq. 2.10 can be extended to reflect X-ray attenuation by both tissues,

$$\frac{I}{I_0} = \exp\left(-\mu_B D_B - \mu_S D_S\right) \tag{2.16}$$

where μ_B is the X-ray absorption coefficient for compact bone and μ_S is the soft tissue absorption coefficient. It is assumed that the X-ray travels a total length D_B in compact bone and D_S in soft tissue, irrespective of the order of the tissues (such as, for example soft tissue—bone—soft tissue). Usually, D_S is not known and X-ray absorption by soft tissue causes a higher apparent bone density. The unknown absorbance can be eliminated by measuring the intensity at two different energies along the same path. The X-ray attenuation coefficients are energy-dependent (Fig. 2.10), and two different intensities I_H and I_L are obtained from high- and low-energy X-rays, respectively:

$$\begin{aligned} I_H &= I_0 \exp\left(-\mu_{B,H} D_B - \mu_{S,H} D_S\right) \\ I_L &= I_0 \exp\left(-\mu_{B,L} D_B - \mu_{S,L} D_S\right) \end{aligned} \tag{2.17}$$

When the incident intensity is known, for example, from an X-ray path through air, the intensities in Eq. 2.17 can be converted into total absorbance A_H and A_L, respectively:

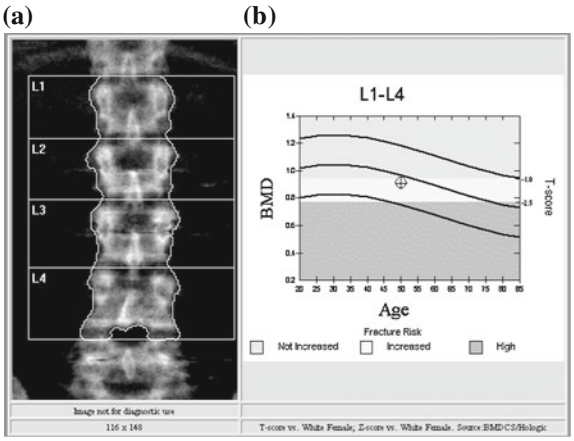

Fig. 2.13 DEXA scan of the lumbar spine. Lumbar vertebrae L1 through L4 haven been segmented by the software (**a**), and bone density is determined for the outlined regions. Since density is averaged for each vertebra, the low spatial resolution seen in the AP projection is acceptable for DEXA. The software also displays the average density in relation to a standard cohort (**b**). The three lines indicate mean bone density over age (*central line*) and the standard deviation of the cohort (*upper and lower lines*). Bone density for this patient was found to be slightly below the age-matched mean. *Image* © Springer Verlag, 2011, from Haidekker MA & Dougherty G, in: Medical Image Processing: Techniques and Applications, Springer 2011

$$\begin{aligned} A_H &= \mu_{B,H} D_B + \mu_{S,H} D_S \\ A_L &= \mu_{B,L} D_B + \mu_{S,L} D_S \end{aligned} \tag{2.18}$$

The unknown quantity D_S can now be removed from the absorbance image A by computing a weighed difference of both absorbances,

$$A = \mu_{B,H} D_B + \mu_{S,H} D_S - w \left(\mu_{B,L} D_B + \mu_{S,L} D_S \right) \tag{2.19}$$

where w needs to be chosen as

$$w = \frac{\mu_{S,H}}{\mu_{S,L}} \tag{2.20}$$

Like conventional X-ray imaging, DEXA is a projection imaging method. Image analysis steps consist of the automated detection of the bone region and the computation of the averaged density. An example is shown in Fig. 2.13. DEXA is typically applied to the thoracic or lumbar spine, the femoral neck, or the calcaneus.

The accuracy of the DEXA method is limited for two main reasons. First, the absorption coefficients are approximations, because the X-ray beam is polychromatic. Second, and more importantly, the premise of the DEXA model is a two-tissue system (bone and soft tissue). However, soft tissue may be composed of muscle and adipose tissue, and the absorption values $\mu_{S,H}$ and $\mu_{S,L}$ show variability between individuals. In spite of these errors, DEXA typically shows a measurement accuracy of 10 % or better compared to ash mass [9].

2.3 X-Ray Detectors

X-ray intensity can be measured with photographic film or with digital detectors. Film, due to its simplicity, its high dynamic range, and its high spatial resolution is still commonly used, although direct digital acquisition becomes more and more widespread. Both film and electronic detectors have in common a low quantum efficiency. Most X-ray photons would pass through film, for example, rather than causing the chemical reaction that leads to blackening of the film. Scintillation crystals exist that convert X-ray photons into—depending on the application—visible or UV photons. Scintillation crystals are therefore used in conversion layers to absorb X-rays with a high efficiency and produce those low-energy photons for which the detectors show a high sensitivity.

2.3.1 Film-Based Imaging

Photosensitive film uses silver halide salts (usually $AgBr_2$) as the photosensitive compound. The silver halide is embedded in a thin, water-permeable layer (the *emulsion*). When exposed to visible or UV light, the salt breaks apart, and a *latent image* of elemental silver emerges. Two processing steps are necessary to create the final image. First, a developer (an aqueous, alkaline solution of several organic compounds) breaks apart more silver halide near the initial atoms of elemental silver. The elemental silver is responsible for the darkening (i.e., the high light absorption) of the exposed parts of the film. Second, a fixation solution (its central chemical is an inorganic thiosulfate) removes the remaining silver halide and prevents further darkening. Thorough rinsing is necessary to remove the development chemicals. The entire development process is usually performed by automated development machines—up to the level where the film is removed from the cassette by the machine, thus making a darkroom unnecessary (daylight processing).

For mechanical stability, the emulsion layer is supported by a transparent polymer film, the *carrier* (Fig. 2.14b). A thin, water-permeable layer mechanically protects the film on the emulsion side. Film has a very high dynamic range with light attenuation in the darkest regions of 1:1000 or higher. Some films have emulsion layers on both sides, effectively doubling their dynamic range.

Since film is sensitive towards light in the visible or UV range, the X-ray photons need to be converted. For this purpose, the film is placed in a cassette in close proximity to a conversion layer (Fig. 2.14a). Traditionally, tungsten compounds have been used, but newer materials based on rare earth metals show a higher efficiency (Table 2.3). Particularly, the high quantum yields of the rare earth materials allow a significant reduction of the patient dose. Calcium tungstate, for example, requires about three times the dose of terbium-doped gadolinium oxysulfide (Gd_2O_2S:Tb) to emit the same amount of light. The large difference in the absorption coefficient of

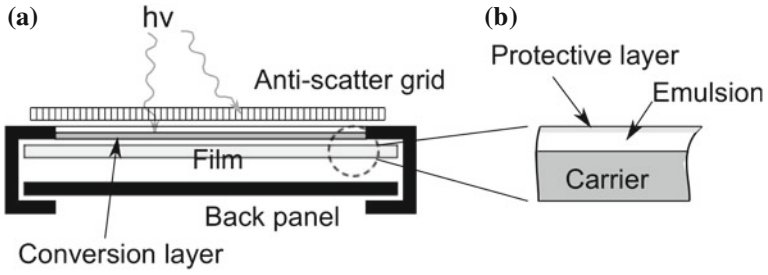

Fig. 2.14 Sketch of an X-ray film cassette (**a**) and photosensitive film (**b**). The cassette itself is a sturdy metal box with a removable panel to allow easy insertion of the photosensitive film. Most importantly, the cassette features a conversion layer, often on a glass support, that absorbs X-rays and emits visible or UV light. Film itself is composed of an emulsion layer that contains the photosensitive silver, applied onto a transparent polymer carrier

Table 2.3 X-ray absorption coefficient μ and quantum yield of some conversion layer materials

Conversion material	Absorption coefficient (mm^{-1})		Quantum yield (%)	Emission range
	at 40 keV	at 80 keV		
$CaWO_4$	4.00	3.15	4	Blue
LaOBr : Tb	13.1	1.86	13	Blue
Gd_2O_2S : Tb	4.62	3.29	19	Green

lanthanum oxybromide (LaOBr:Tb) between 40 and 80 keV can be explained with the presence of a k-edge slightly below 40 keV.

In a wide exposure range, film darkening follows a power-law relationship with the exposure. Since the human senses have logarithmic responses, film density is usually measured with the unitless logarithmic *optical density* OD, defined as

$$\mathrm{OD} = -\log_{10} T = \log_{10} \frac{I_0}{I} \tag{2.21}$$

where T is the transmission, that is, the fraction I of the incident illumination I_0 that is not absorbed by the film. We can approximately describe the film response to the X-ray exposure E as

$$OD = C \cdot \log E \tag{2.22}$$

where C is the film's contrast. However, in both the high exposure range and the low exposure range, the film deviates from Eq. 2.22, and a typical film sensitivity curve is shown in Fig. 2.15. The film carrier and the emulsion are not perfectly clear. Films used in diagnostic radiology transmit about 78 % of the incident light (optical density of 0.11) when unexposed. Minor blackening of the film remains invisible against the natural fogginess of the carrier/emulsion system. Radiologists refer to the region of underexposure in the sensitivity curve as the *toe region* of the film. Conversely, there is an exposure level where all available silver halide has been converted to elemental

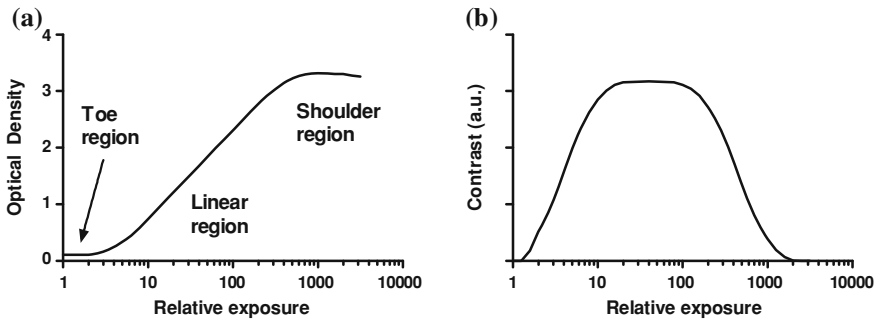

Fig. 2.15 Sensitivity curve **a** and contrast curve **b** of typical photographic film used in diagnostic radiology. In the toe region, very weak blackening cannot be seen in the natural fog and base absorption of the film. In the shoulder region, all available silver has been converted, and increased exposure does not lead to further blackening. A linear region between toe and shoulder exists. The film contrast is the first derivative of the sensitivity

silver, and further exposure does not increase blackening. This saturation region is called the *shoulder region.*

A wide variety of radiological films is available for any specific purpose. Films can be sensitized toward special conversion layers (for example, blue-or green-sensitive films), and films with different contrast are available. High-contrast films have a very narrow linear region and need to be accurately exposed. Films with lower contrast are good for general-purpose imaging and scout images. The region of optimal contrast (i.e., the region between toe and shoulder) is called the film's *latitude*. High-contrast films have a lower latitude than low-contrast films.

2.3.2 Fluoroscopes

The invention of the fluoroscope was the first major step in the direction of lower patient exposure and lower exposure times. Initially, a fluoroscope was a conversion layer (such as calcium tungstate) mounted in front of a light-shielded observation box. The radiologists used the fluoroscope to make the X-rays visible, but were exposed to the primary X-rays in the process. Development of image intensifiers remedied this situation.

Image intensifiers are based on a special photocathode composed of two conversion layers. The first layer is cesium iodide (CsI), which acts similar to the conversion layers in film cassettes, i.e., it emits visible light when hit by X-ray photons. However, cesium iodide has a very high quantum yield, producing about 3000 visible-light photons per X-ray photon (at 60 keV). Cesium iodide has the additional advantage of forming elongated crystals, and these crystals act as a form of natural anti-scatter grid. The second layer of the photocathode, often combinations of metals with antimony salts (Sb_2S_3), emits electrons when exposed to the visible light coming from

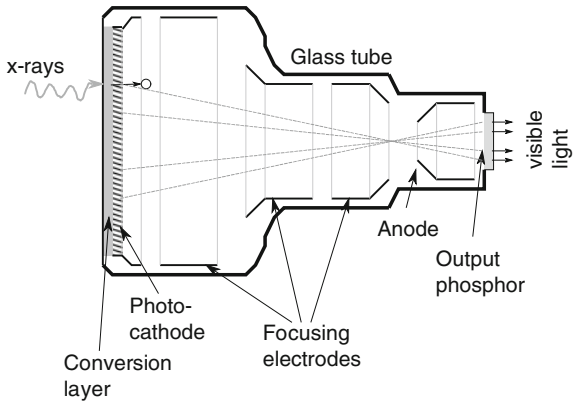

Fig. 2.16 Schematic representation of an electronic image intensifier. A conversion layer strongly absorbs X-ray photons and emits electrons. The electrons are accelerated and focused onto a luminescent output phosphor. The output window therefore displays a scaled-down and inverted image by visible-light emission. The image can be monitored in real-time with a TV camera and monitor

the CsI input layer. In vacuum, these electrons can be accelerated and directed onto a phosphor screen that is somewhat similar to the screen of a monochrome TV set, i.e., it emits visible light when hit by electrons. One example for an output phosphor material is ZnCdS:Ag, which emits green light when hit by kinetic electrons.

Figure 2.16 shows the principle of an image intensifier. A photocathode, preceded by a cesium iodide conversion layer, emits electrons when hit by an X-ray photon. These electrons are accelerated in an electrostatic field toward the anode. Typical acceleration voltages are 15–25 kV, similar to CRT TV tubes. A series of focusing electrodes ensures a highly defined path of the electrons such that each point on the input window is mapped to a point on the output window. For this reason, the output phosphor displays the image projected with X-rays onto the input conversion layer, but at a smaller scale and inverted. In addition, some geometric distortion occurs, and the output image is blurred to some extent. However these disadvantages are outweighed by the very high sensitivity of the image intensifier, which allows recording of the image in real-time, that is, at video frame rates. When the output phosphor is coupled to a video camera, the image can be monitored in a separate room.

Image intensifiers are fundamental for interventional radiology and image-guided surgery. In both situations, the patient is continuously monitored under low-dose X-ray illumination. X-ray source and image intensifier are mounted on a C-shaped arm, which allows flexible positioning with respect to the patient.

Moreover, fluoroscopy with image intensifiers allows special procedures, such as digital subtraction angiography, where an image before the injection of a contrast agent is subtracted from an image after contrast agent injection. The result is an image that displays only the contrast material-filled blood vessels and allows excellent visibility of the blood vessels. A change of the potentials on the focusing electrodes

allows to reduce the field of view and therefore enter a magnification mode that makes even smaller details visible.

More recently, image intensifiers as sketched in Fig. 2.16 are more and more often replaced by semiconductor-based intensifiers, which can have an even higher quantum efficiency combined with lower spatial distortion, but semiconductor (flat-panel) intensifiers are still more expensive.

2.3.3 Semiconductor Detectors

Semiconductor detectors for digital radiology work analogously to film and the electronic fluoroscope: A conversion layer captures the X-rays with high quantum efficiency and gives off visible light, which in turn is captured by conventional visible light detectors, such as CCD (charge-coupled devices) and CMOS arrays. The basic light-sensitive element in a CCD detector is remotely related to a field-effect transistor with a metal-oxide gate. The main difference is the photosensitivity. Silicon p–n junctions are inherently sensitive to light, because a photon in the visible-light energy range can generate an electron-hole pair by elevating an electron from the valence band to the conduction band (photoelectric effect in semiconductors). In the special case of a CCD sensor, the channel under the gate is exposed to light. Electron-hole pairs are generated by light exposure, and the negative charges are held—and accumulated—under the influence of a positive gate potential. The process of exposure with charge accumulation and subsequent read-out is explained in Fig. 2.17. At the end of the channel, a charge amplifier and an A/D converter provide a digital signal that is proportional to the light exposure. CMOS sensors, which are more common than CCD sensors in low-end applications, follow a similar principle, but have added per-pixel processing circuitry at the expense of light sensitivity. For X-ray detection, the detector chip (CCD or CMOS) is sandwiched with a conversion layer. Unlike electronic image intensifiers, CCD-based semiconductor detectors are flat—even thinner than a film cassette. Unlike image intensifiers, spatial resolution can be very high. In fact, CCD chips with 10 μm pixel size or smaller are common. With a suitable microfocus X-ray tube, this gives rise to X-ray microscopy. On the other hand, CCD-based X-ray detectors generally do not achieve the sensitivity of image intensifiers, and a lower dose requires longer exposure times and simultaneously adds a strong noise component to the image.

Sensitivity can be increased by using the avalanche principle. In an avalanche diode, a low-doped intrinsic region is placed between the p- and n-Si zones (this configuration is called *pin-diode*). The intrinsic barrier allows the diode to be reverse-biased with high voltages of 100–200 V. Charges created in the junction zone by photoelectric absorption are accelerated by the high potential field and release additional charges along their path (thus, avalanche). Avalanche diodes are relatively large and require additional supporting circuitry. Although they can feature very high sensitivity, the spatial resolution is generally low, and avalanche diode imaging arrays are still a subject of active research.

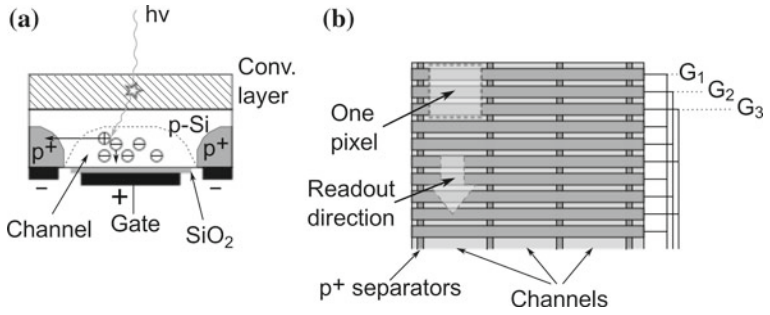

Fig. 2.17 Schematic of a charge-coupled device (CCD). The cross-section of a single element (pixel) is shown in **a**. In weakly doped p-Si, a n-channel is created by applying a positive voltage to a MOS gate. X-ray photons are captured by a conversion layer that is grown directly on top of the light-sensitive silicon wafer. The conversion layer emits visible light, which is captured by the silicon and creates an electron-hole pair. Electrons are captured and therefore accumulated in the positive gate field during the exposure, whereas holes (positive carriers) are shunted into the p^+ regions that separate the channels. **b** shows a view from the MOS gate side. Every third gate is connected. During exposure, only G_2 has a positive potential. During the read-out phase, a potential is applied to G_3, and the negative charges are attracted to the zone underneath G_3 and therefore move downward. Next, the positive potential is applied to G_1. Thus, the packet of accumulated charges is transported to the end of the CCD array, where it is read out. Each cycle G_2–G_3–G_1 allows to read out one row of pixels

2.3.4 Photomultiplier Tubes

The ultimate detection device when it comes to sensitivity is the photomultiplier tube (PMT). PMTs are high-voltage vacuum devices, somewhat like the electronic image intensifier. A PMT consists of several electron-multiplying *dynodes*. As shown in Fig. 2.18, an X-ray photon is absorbed by the conversion layer and converted into visible light. A visible-light photon that enters the PMT and hits the photocathode releases an electron—the photocathode is functionally similar to the photocathode of the image intensifier. This electron is accelerated in an electrostatic field toward the first dynode. In the process, the electron reaches a sufficiently high kinetic energy to release multiple electrons from the dynode it hits. These multiple electrons are now accelerated toward the second dynode, where *each* electron now releases multiple electrons, which in turn are accelerated towards the next dynodes. At the end of the dynode chain, the electrons are captured by the anode and create a measurable current spike *per photon* that hits the photocathode. Typical PMTs have 10 dynodes (multiplying stages), and each dynode releases between 3 and 5 electrons per received electron. Each photon can therefore cause a charge of 10 million electrons (1.5 pC) to be deposited on the anode, causing a pulse of several nanoamperes for a microsecond. The multiplication factor, that is, the average number of secondary electrons released per primary electron at any dynode is determined by the voltage difference between dynodes. Typically, a voltage divider creates the voltage gradient from the cathode to the anode, and by adjusting the cathode voltage, the overall sensitivity is controlled.

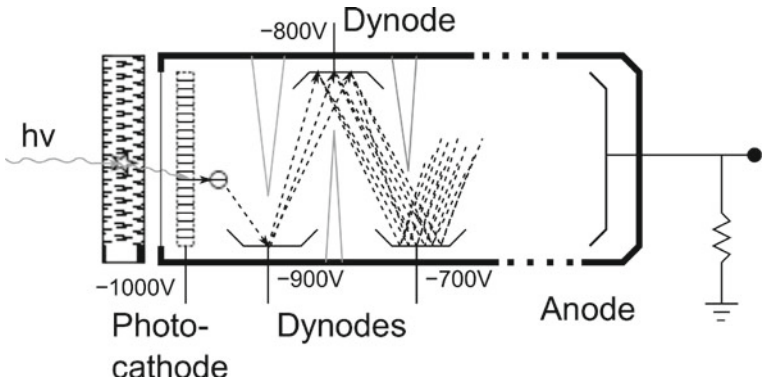

Fig. 2.18 Schematic of a photomultiplier tube (PMT). The light-sensitive part is very similar to the electronic image intensifier (Fig. 2.16) as an X-ray photon is converted into visible light, which in turn hits the photocathode, where an electron is released into the vacuum. This electron is accelerated toward the first dynode, where it gathers enough energy to release 3–5 secondary electrons from the dynode upon impact. These secondary electrons are accelerated toward the next dynode where the process is repeated. After several multiplying stages (i.e., dynodes), a measurable electron shower hits the anode

PMTs can be operated in a lower-sensitivity continuous mode, where the anode current is proportional to the photon flux at the photocathode, or in the higher-sensitivity *photon-counting* mode. In photon-counting mode, the current pulse that is caused by each photon at the anode is measured and counted. PMTs operating in photon-counting mode can easily be saturated (*pulse pile-up*), and in this mode, a PMT should not be operated above a flux 10^6 photons per second, because a strong deviation from linearity can be expected. High-sensitivity PMTs can be damaged by overexposure to light.

A very detailed insight into principles and practice of photomultiplier tubes can be gained from R.W. Engstrom's *Photomultiplier Handbook* [10], which is freely available on the web.

PMTs are relatively large, with optical windows between 5 and 50 mm. Therefore, any detector that relies on PMTs has a very low spatial resolution. However, this is a price worth paying when extremely low radiation doses are required, typically in nuclear medicine. In Chap. 4, we will see that PMTs are fundamental elements in the γ-sensitive *Anger camera* for SPECT (single-photon emission computed tomography) and for γ-detection in PET (positron emission tomography).

2.4 Factors that Determine X-Ray Image Quality

We have already encountered two factors that degrade X-ray image quality, *blur* and *haze*. Noise is an additional factor, notably in digital detection systems. In this section, the most important factors that cause image degradation are summarized.

- Geometric blur. Geometric blur occurs when details are imaged that are smaller than the X-ray beam diameter. The primary factor is the size of the focal spot, since the image is a convolution of the imaged object with the intensity distribution along the focal spot. Selectable focal spot sizes or special microfocus tubes help control geometric blur. Furthermore, keeping the object (patient) close to the detector also reduces geometric blur.
- Detector blur. Detector blur is caused by the conversion layer. The conversion layer typically emits visible light with equal probability in all directions. With a thick conversion layer, cross-talk between neighboring pixels is possible (whereas a thin conversion layer has a lower quantum efficiency). Keeping the conversion layer as close to the detector element as possible reduces detector blur.
- Motion blur. Motion blur occurs when the patient moves during exposure, for example by breathing. Generally, high detector sensitivity and high photon flux from the X-ray source allow shorter exposure times and reduce motion blur.
- Haze. Haze is primarily caused by scattered X-ray photons (Compton scattering). An anti-scatter grid reduces the amount of off-angle photons. For thin layers of tissue (e.g., the extremities), a lower X-ray energy can increase the influence of photoelectric absorption and Rayleigh scattering and thus decrease haze.
- Nonlinearity, over-and underexposure. Both over- and underexposure reduce image contrast. Overexposure applies equally to film and electronic detectors. Underexposure is more critical in electronic detectors due to the higher noise floor. Prior experience and—if necessary—a scout image can help selecting the correct exposure. The optical density of a film generally depends on the exposure in a nonlinear fashion. The use of calibration phantoms of known density allow per-image calibration.